

How Semilocal Are Semilocal Density Functional Approximations? —Tackling Self-Interaction Error in One-Electron Systems

Akilan Ramasamy,¹ Lin Hou,^{1,2} Jorge Vega Bazantes,¹ Tom
J. P. Irons,³ Andrew M. Wibowo-Teale,^{3,4} and Jianwei Sun^{1,*}

¹*Department of Physics and Engineering Physics,
Tulane University, New Orleans, Louisiana 70118, USA*

²*Theoretical Division, Los Alamos National Laboratory, Los Alamos, New Mexico 87545, USA*

³*School of Chemistry, University of Nottingham,
University Park, Nottingham NG7 2RD, United Kingdom*

⁴*Hylleraas Centre for Quantum Molecular Sciences, Department of Chemistry,
University of Oslo, P.O. Box 1033, N-0315 Oslo, Norway*

(Dated: November 22, 2024)

Self-interaction error (SIE), arising from the imperfect cancellation of the spurious classical Coulomb interaction between an electron and itself, is a persistent challenge in modern density functional approximations. This issue is illustrated using the prototypical one-electron system H_2^+ . While significant efforts have been made to eliminate SIE through the development of computationally expensive nonlocal density functionals, it is equally important to explore whether SIE can be mitigated within the framework of more efficient semilocal density functionals. In this study, we present a non-empirical meta-generalized gradient approximation (meta-GGA) that incorporates the Laplacian of the electron density. Our results demonstrate that the meta-GGA significantly reduces SIE, yielding a binding energy curve for H_2^+ that matches the exact solution at equilibrium and improves across a broad range of bond lengths over those of the Perdew-Burke-Ernzerhof (PBE) and strongly-constrained and appropriately-normed (SCAN) semilocal density functionals. This advancement paves the way for further development within the realm of semilocal approximations.

Kohn-Sham density functional theory (KS-DFT) [1] is a widely used quantum mechanical method in condensed-matter physics and quantum chemistry due to its balance of computational efficiency and accuracy. DFT reduces the complexity of many-electron systems by describing their ground-state properties in terms of the electron density, rather than the many-body wavefunction [2], significantly lowering the computational cost. It is exact in theory for a system of electrons under an external potential typically generated by nuclei with the total electronic energy being given by,

$$E[n] = T_s[n] + E_H[n] + E_{en}[n] + E_{xc}[n] \quad (1)$$

where $n(r)$ is the electron density, $T_s[n]$ the kinetic energy, $E_H[n]$ the Hartree energy, $E_{en}[n]$ the electron-nuclei interaction, and $E_{xc}[n]$ the exchange-correlation energy. However in practice the exchange-correlation (XC) energy functional, $E_{xc}[n] = E_x[n] + E_c[n]$ has to be approximated as its exact form in terms of $n(r)$ is not explicitly known.

One of the most significant challenges in widely used density functional approximations (DFAs) is the self-interaction error (SIE) [3], which arises from the inability of these approximations to fully cancel the spurious classical Coulomb interaction of electron with itself. For example, for any one electron system, there is no electron-electron interaction, and thus the correlation energy should be zero, $E_c[n] = 0$, and the exchange energy

should exactly cancel out the Hartree energy, $E_x[n] = -E_H[n]$. The Hartree-Fock (HF) method satisfies these conditions exactly and proves to be an exact method for describing all one-electron systems.

However, this is typically not the case for DFAs, in particular for the widely used efficient semilocal approximations. SIE in DFAs can lead to inaccuracies in predictions of properties such as bond dissociation energies, transition states, magnetic properties, and band gaps [4–14]. Over the years, various methods like Perdew-Zunger self-interaction correction (PZ-SIC) and its variant [3, 15–17], localized orbital scaling correction (LOSC) [18, 19], local hybrid density functionals [20–22], and other nonlocal density functionals [23–25] have been developed to reduce or eliminate SIE, offering improvements but often at the cost of increased computational demands due to their nonlocal nature.

Therefore, it is equally important to evaluate how well semilocal density functional approximations (DFAs) handle SIE due to their computational efficiency. This is especially relevant given the success of the Strongly Constrained and Appropriately Normed (SCAN) [26] functional, which has shown significant improvements over the Perdew-Burke-Ernzerhof (PBE) [27] functional across a wide range of materials and properties [28]. SCAN achieves these advancements partially by reducing SIE within the semilocal framework [11–14], as shown in Figure 1 of the prototypical H_2^+ binding energy curve, which is commonly used to define and illustrate SIE. This raises an intriguing question: can SIE be further minimized while retaining the computational efficiency of semilocal DFAs? Addressing this challenge could lead

* Correspondence email address: jsun@tulane.edu

to the development of even more accurate and efficient functionals, expanding their utility across various applications.

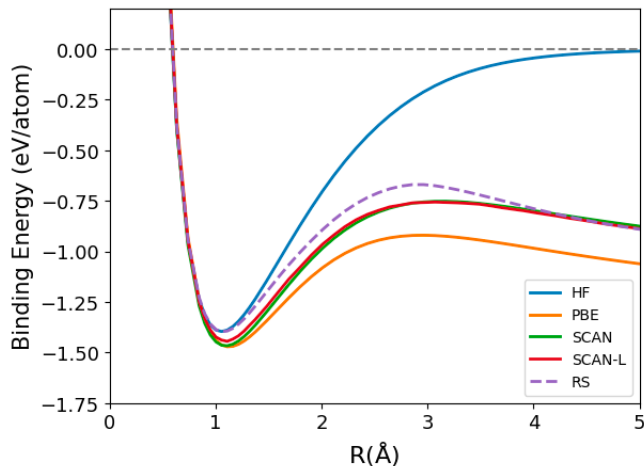


Figure 1. H_2^+ binding energy curves of HF and exchange-only density functionals evaluated on HF orbitals.

In this letter, we present a positive answer to this critical question by introducing a non-empirical semilocal density functional that depends on the Laplacian of the electron density. As shown in Figure 1, this newly designed functional, referred to as RS, significantly reduces SIE, demonstrating clear improvements over other semilocal DFAs like SCAN and PBE in the H_2^+ binding energy curve.

Semilocal DFAs can be written as,

$$E_{xc}[n] = \int d^3\mathbf{r} n \epsilon_{xc}(n, \nabla n, \nabla^2 n, \tau). \quad (2)$$

In local density approximation (LDA) [29, 30], the electron density, $n(\mathbf{r})$ is the only ingredient. Generalized gradient approximations (GGA) [27, 31, 32] add the electron density gradient, ∇n . Meta-GGAs [26, 33–40] further include the Laplacian of electron density, $\nabla^2 n$, and/or the kinetic energy density, $\tau = \frac{1}{2} \sum_{i=1}^{N_{\text{occ}}} |\nabla \phi_i|^2$, where ϕ_i are Kohn-Sham orbitals. With more ingredients, semilocal DFAs can satisfy more exact constraints, which are the known properties of the exact exchange-correlation energy [26, 41].

SCAN is a metaGGA that doesn't depend on $\nabla^2 n$ and uses τ to identify different chemical environments through the variable $\alpha = (\tau - \tau^W)/\tau^{unif}$ with $\tau^W = |\nabla n|^2/8n$ and $\tau^{unif} = (3/10)(3\pi^2)^{2/3}n^{5/3}$ [42]. The τ -dependence also allows SCAN to satisfy all 17 exact constraints suitable for semilocal functionals, including those for iso-orbital (one- and two-electron) systems that are not amenable to GGAs. Moreover, it provides the flexibility to guide the functional between exact constraints using appropriate norms, for example, the hydrogen atom, whose exchange-correlation holes are localized and deep [26].

Meta-GGAs that depend on $\nabla^2 n$ can be derived by de-orbitalizing τ -dependent meta-GGAs, by replacing τ with a function of $\nabla^2 n$ that offers faster computations. The SCAN-L functional [37] is a de-orbitalized version of SCAN, and it demonstrates surprisingly comparable accuracy for many systems and properties [37, 43], including the binding energy curve of H_2^+ , as shown in Figure 1. However, since α is only approximated by the de-orbitalized $\alpha_L(\nabla^2 n)$, SCAN-L only approximately satisfies many of the exact constraints that SCAN obeys. For instance, SCAN-L is not self-correlation free in one-electron systems. Furthermore, de-orbitalization does not guarantee that SCAN-L will be accurate for all appropriate norms. As shown in Table I, SCAN-L underestimates the exchange energy of the hydrogen atom in magnitude.

For one-electron systems, $\tau = \tau^W = \frac{|\nabla n|^2}{8n}$, and the SCAN meta-GGA loses its dependence on τ and thus reduces to a GGA. In contrast, SCAN-L remains a meta-GGA, still dependent on $\nabla^2 n$. Interestingly, the inclusion of this additional ingredient does not improve SCAN-L over SCAN for the binding energy curve of H_2^+ , and even worsens its performance for the exchange energies of two analytically known one-electron densities in Table I, namely H and the Gaussian electron density (G). This raises a question: can SIE be further reduced in one-electron systems by properly incorporating $\nabla^2 n$ into the functional design, while still satisfying exact constraints and being guided by appropriate norms? Addressing this question would also provide insight into reducing SIE within the semilocal approximation framework, as the τ -dependence could be layered on top of the $\nabla^2 n$ -dependence at the meta-GGA level.

To address this question, we start with the $\nabla^2 n$ -dependent meta-GGA exchange energy of a spin-unpolarized density,

$$E_x^{MGA}[n] = \int d^3\mathbf{r} n \epsilon_x^{unif} F_x(s, q) \quad (3)$$

where $\epsilon_x^{unif} = -(3/4\pi)(3\pi^2 n)$ is the exchange energy per particle of a uniform electron gas. $F_x(s, q)$ is the exchange enhancement factor depending on two dimensionless ingredients, the reduced density gradient $s = |\nabla n|/[2(3\pi^2)^{1/3}n^{4/3}]$ and the reduced electron density Laplacian $q = \nabla^2 n/[4(3\pi^2)^{2/3}n^{5/3}]$. The exchange energy for any spin-polarized density can be found from the exchange energy of a spin-unpolarized density using the exact spin-scaling relationship [44]. We don't consider the correlation energy functional in this study as τ -dependent metaGGAs can be made one-electron self-correlation free [26, 34].

For one-electron systems, the SCAN meta-GGA reduces to a GGA, with

$$F_x^{SCAN}(s) = 1.174 \left(1 - e^{-\frac{s}{\sqrt{s}}}\right). \quad (4)$$

By design, $F_x^{SCAN} \geq 0$, satisfying the exact constraint of exchange energy being negative [45], $F_x^{SCAN} \leq 1.174$,

satisfying the tight Lieb-Oxford bound for any one-electron densities [46], and $F_x^{SCAN} \rightarrow s^{-1/2}$ as $s \rightarrow \infty$, satisfying the finite exchange energy per electron under the one-dimensional, nonuniform coordinate scaling [47]. The parameter $a = 4.9479$ is then determined by the exchange energy of H. The resulting $F_x^{SCAN}(s)$ decreases monotonically with s , providing greater enhancement for electron densities with small s , which are typically more compact and slowly varying, than those with large s that are dilute and rapidly varying. Such a simple construction works surprisingly well for one-electron systems, improving over PBE, as demonstrated in Table I for H and Gaussian electron density and Figure 1 for H_2^+ . It is thus desirable to keep this simplicity when introducing the q dependence into $F_x(s, q)$.

Table I. Comparison of exchange energies (in Ha) of different functionals for H and Gaussian electron densities.

System	LSDA	PBE	SCAN	SCAN-L	RS	Exact
Hydrogen	-0.2680	-0.3059	-0.3125	-0.3110	-0.3125	-0.3125
Gaussian	-0.3410	-0.3819	-0.3975	-0.3965	-0.3989	-0.3989

We therefore design our RS metaGGA by coupling the enhancement factor of SCAN with a function $g(s, q)$,

$$F_x^{RS}(s, q) = 1.174 \left(1 - e^{-\frac{a}{\sqrt{s}}}\right) \cdot g(s, q), \quad (5)$$

where

$$g(s, q) = \left(\frac{1}{1 + \ln(1 + e^{b \cdot (q - q_0(s))})} \right). \quad (6)$$

Here, a , b , and $q_0(s)$ are two free parameters and a function of s , respectively, which will be determined by appropriate norms to be discussed later. By construction, $0 \leq g(s, q) \leq 1$ for any $s \geq 0$ and $-\infty \leq q \leq \infty$. This guarantees that RS satisfies the exact constraints of exchange energy being negative and the tight Lieb-Oxford bound for any one-electron densities.

$g(s, q)$ is also designed to monotonically decrease with q , in view of the success of $F_x^{SCAN}(s)$ being monotonically decreasing with s which was discussed earlier. This requires $b > 0$. According to Bader's theory of atoms in molecules (AIM) [48], the behavior of $\nabla^2 n$ provides critical insights into electronic structure. In regions of high electron density, such as at bond centers for compressed or equilibrium bonds and at nuclei, $\nabla^2 n$ is negative. Conversely, in regions of low electron density, including inter-shell regions and bond centers of highly stretched bonds, $\nabla^2 n$ becomes positive. For example, as the bond of H_2^+ is stretched, q at the bond center becomes more positive (see section II in Supplementary Material).

For an electron density under the one-dimensional, nonuniform coordinate scaling, $q \rightarrow -\infty$ for some region

as the coordinate scaling strength goes to ∞ , and $q \rightarrow \infty$ for the other region (see section III in Supplementary Material). In the region where $q \rightarrow -\infty$, $g(s, q) \rightarrow 1$, while for the other region, $q \rightarrow \infty$, $g(s, q) \rightarrow 0$. Therefore, $g(s, q)$ guarantees that F_x^{RS} reduces to F_x^{SCAN} for the $q \rightarrow -\infty$ region, and 0 for the other region, yielding a finite exchange energy for one-electron systems under the one-dimensional, nonuniform coordinate scaling.

The appropriate norms used here to determine a , b , and $q_0(s)$ are H and Gaussian electron density, which have analytic expressions (see section IV of Supplementary Material). Figure 2 (a) shows the system- and spherically-averaged exchange hole [49, 50] against the inter-electron distance, u , for H and Gaussian electron density along with H_2^+ at various bond lengths. In comparison to H, Gaussian electron density as well as H_2^+ with the bond length, $R \leq 1.058 \text{ \AA}$ have deeper exchange holes, while H_2^+ with the bond length, $R \geq 1.270 \text{ \AA}$ have shallower ones. It suggests that Gaussian electron density is as qualified for being an appropriate norm as H for semilocal density functionals since Gaussian electron density is also analytically known and not related to bonding. From the comparison between the PBE exchange holes and the exact ones given in section V of Supplementary Material, it is obvious that PBE's exchange holes are more short-ranged than the exact ones, and become too deep for large bond lengths R of H_2^+ . It is also interesting to note that although the exact exchange holes of H_2^+ at equilibrium ($R = 1.058 \text{ \AA}$) and Gaussian electron density are deeper than those of H, SCAN predicts an overly negative exchange energy for the former (see Figure 1) and a less negative one for the latter (see Table I). This suggests that the tailored GGA (eq. 4) may be limited by its variables and could benefit from incorporating q for improved accuracy.

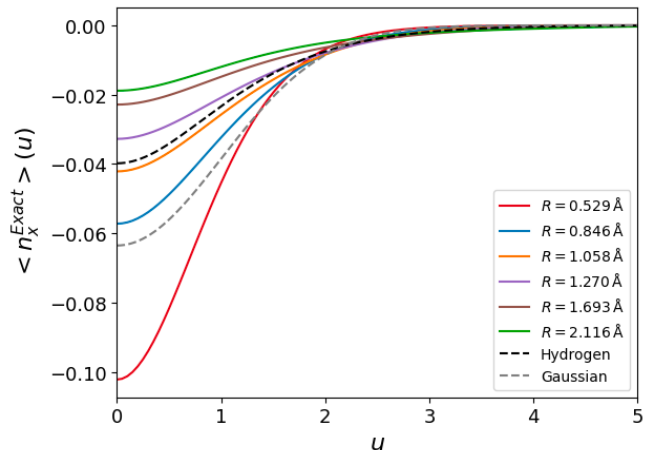


Figure 2. System- and spherically-averaged exact exchange holes plotted against the inter-electron distance u for H, Gaussian electron density, and H_2^+ with various bond lengths.

To match the exact exchange energies of the appropriate norms, i.e., H and Gaussian electron density, incorpo-

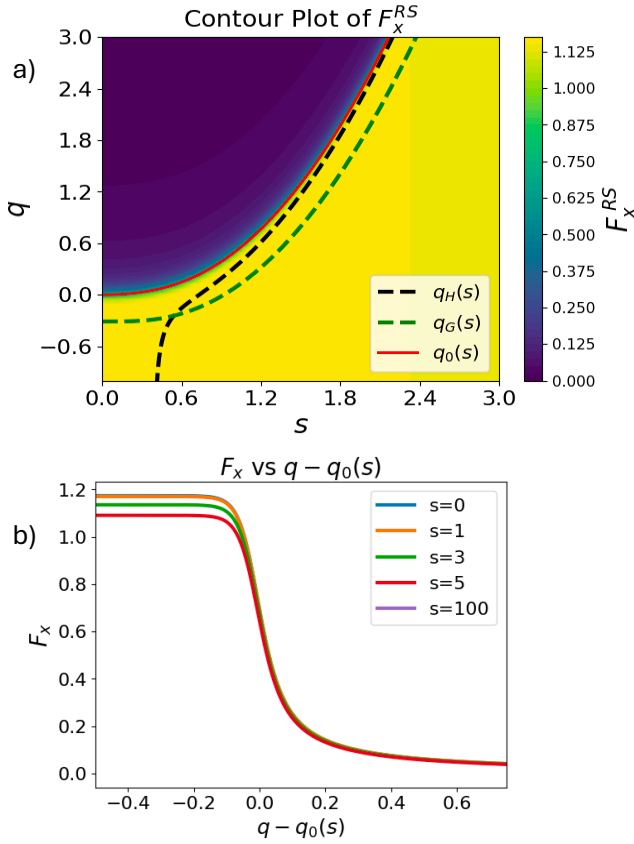


Figure 3. (a) Contour Plot of the RS enhancement factor against s and q . (b) Enhancement factor of RS as a function of $(q - q_0(s))$ for various values of s .

rating q -dependence through $g(s, q)$ in the RS meta-GGA requires careful design of the function $q_0(s)$. Because of the spherical symmetry and monotonicity in electron density, $q(r)$ of H and Gaussian electron density can be expressed as functions of $s(r)$, and we denote them as $q_H(s)$ and $q_G(s)$, plotted in Figure 3 (a) as black and green dashed lines, respectively. For most of the regions, $q_G(s) < q_H(s)$. $q_H(s)$ has an analytical form (see section VI of the Supplementary Material for the derivation),

$$q_H(s) = s^2 \left[1 - \frac{2}{3 \ln((6\pi)^{1/3} s)} \right] \quad (7)$$

Our choice of $q_0(s)$ is a modification of $q_H(s)$,

$$q_0(s) = s^2 \left[1 - \frac{2}{3 \ln((6\pi)^{1/3} (1 + s^2)^{1/2})} \right] \quad (8)$$

by turning s in the denominator into $\sqrt{1 + s^2}$. $q_0(s)$ eliminates the singularity of $q_H(s)$ and approaches $q_H(s)$ asymptotically from above, as shown in Figure 3 (a). This choice of $q_0(s)$ provides the flexibility for $g(s, q) \rightarrow 1$, thereby restoring $F_x^{SCAN}(s)$ for H and Gaussian electron density where $q_H/G(s) - q_0(s) < 0$. For H_2^+ , as the

bond length R increases, q generally becomes more positive (see section II of the Supplementary Material), and thus $F_x^{RS}(s, q)$ tends to decrease as $g(s, q)$ is inversely proportional to q , which is desirable for a less negative exchange energy.

With the designed $q_0(s)$, we determine the parameters $a = 5.93$ and $b = 36.29$ by fitting to the exact exchange energies of H and Gaussian electron density. This parameter set ensures exact matches to the exchange energies of both H and Gaussian electron density, as shown in Table I. Figure 3(b) illustrates that the enhancement factor decays rapidly with q for a fixed s when crossing $q_0(s)$, due to the large value of b . As $q_G(s) - q_0(s) < -0.25$ across most of the s -range in Figure 3(a), Gaussian electron density primarily experiences the form of $F_x^{SCAN}(s)$. Consequently, the parameter $a = 5.93$ is larger than SCAN's 4.9479 to match the exact exchange energy of Gaussian electron density, leading to an enhancement factor that decays more slowly with s than in SCAN.

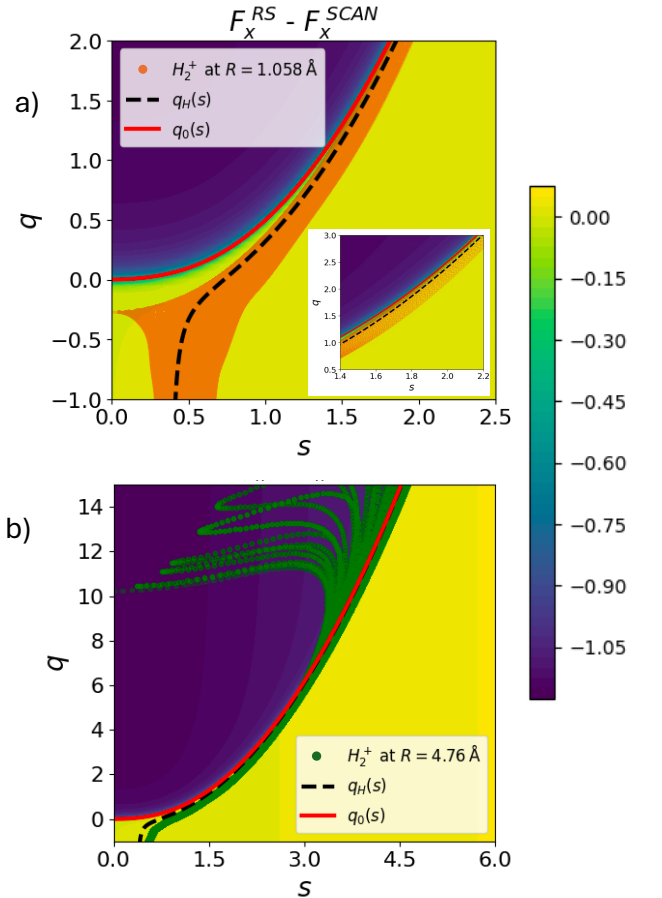


Figure 4. (a) Contour Plot of the difference in the RS and SCAN enhancement factors against s and q , overlaid by (s, q) points existing in H_2^+ at the equilibrium bond length ($R = 1.058 \text{ \AA}$). The inset zooms in the range of $1.4 < s < 2.2$. (b) Same as (a) but for H_2^+ with $R = 4.76 \text{ \AA}$.

Remarkably, this parameter set predicts the total en-

ergy of H_2^+ at equilibrium ($R = 1.058 \text{ \AA}$) to be -0.6026 Hartrees, exactly matching the Hartree-Fock (HF) value. Additionally, the RS binding energy curve aligns perfectly with the HF curve up to slightly beyond $R = 1.058 \text{ \AA}$. This consistency likely reflects the fact that the exchange holes of Gaussian electron densities and H_2^+ (for $R \leq 1.058 \text{ \AA}$) are deeper than those of hydrogen. For stretched bond lengths between $R = 1 \text{ \AA}$ and $R = 3 \text{ \AA}$, the RS binding energy curve shows significant improvement over SCAN and other density functionals. This improvement highlights the importance of incorporating the reduced density Laplacian q in mitigating self-interaction errors.

To understand how RS improves over SCAN for the binding energy curve of H_2^+ , Figure 4 plots (s, q) points existing in H_2^+ at equilibrium ($R=1.058 \text{ \AA}$), overlaid on the contour plot of $F_x^{RS} - F_x^{SCAN}$. There are considerable (s, q) points appear between $q_0(s)$ and $q_H(s)$ lines, and some points with $s > 1.5$ are even above the $q_0(s)$ line, as shown in the inset plot. Given the quick decay of F_x^{RS} vs. $q - q_0(s)$ shown in Figure 3 (b) and the exact match to the exchange energy of H, the above mentioned points have smaller F_x values with RS than with SCAN, resulting in a less negative energy that matches the exact HF energy of H_2^+ at equilibrium as shown in Figure 1. As the bond length increases, for example at $R = 2.116 \text{ \AA}$, more (s, q) points appears above $q_0(s)$, as shown in section VII of Supplementary Material, thereby improving the energy over SCAN.

However, after $R = 4 \text{ \AA}$, the improvement starts to diminish and gets slightly worse than SCAN as shown in Figure 1. This is because the (s, q) points for $R = 4.76 \text{ \AA}$ appearing above $q_0(s)$ have too large q ($q > 6$) as shown in Figure 4(b), associated with relatively small s and very low electron densities (see section II of Supplementary Materials), and become energetically irrelevant. The energetically relevant electron density concentrates

around the atomic centers with (s, q) below $q_H(s)$. This results in more negative exchange energy for RS than for SCAN because F_x^{RS} decays slower than F_x^{SCAN} with s below $q_H(s)$. This is also dictated by the exchange hole of stretched bonds being too shallow, as shown in Figure 2.

In summary, we have developed the non-empirical $\nabla^2 n$ -dependent RS metaGGA that effectively reduces self-interaction errors in one-electron systems, while satisfying all exact constraints for one-electron systems and being guided by appropriate norms. The binding energy of H_2^+ predicted by RS matches the exact HF one beyond the equilibrium point, significantly improving over SCAN across a wide range of bond lengths. The inclusion of $\nabla^2 n$ is shown to be crucial for reducing SIE of H_2^+ at equilibrium and stretched bonds. Our work therefore paves the way for further reducing SIE within the semilocal framework at the metaGGA level while maximally satisfying suitable exact constraints with guidance from appropriate norms.

Acknowledgments: A.R. and J.S. acknowledge the support of the U.S. Office of Naval Research (ONR) Grant No. N00014-22-1-2673. L.H. and J.V.B. were supported by the National Science Foundation (NSF) under Grant No. DMR-2042618, who carried out the calculations related to the exchange holes. The work at Los Alamos National Laboratory was carried out under the auspices of the U.S. Department of Energy (DOE) National Nuclear Security Administration under Contract No. 89233218CNA000001. It was supported by the LANL LDRD Program, and in part by the Center for Integrated Nanotechnologies, a DOE BES user facility, in partnership with the LANL Institutional Computing Program for computational resources. A.M.T. is grateful for support from the European Research Council under H2020/ERC Consolidator Grant “topDFT” (Grant No. 772259).

-
- [1] W. Kohn and L. J. Sham, *Phys. Rev.* **140**, A1133 (1965).
 - [2] P. Hohenberg and W. Kohn, *Phys. Rev.* **136**, B864 (1964).
 - [3] J. P. Perdew and A. Zunger, *Physical review B* **23**, 5048 (1981).
 - [4] A. J. Cohen, P. Mori-Sánchez, and W. Yang, *Science* **321**, 792 (2008).
 - [5] A. Ruzsinszky, J. P. Perdew, G. I. Csonka, O. A. Vydrov, and G. E. Scuseria, *The Journal of chemical physics* **126** (2007).
 - [6] B. G. Johnson, C. A. Gonzales, P. M. Gill, and J. A. Pople, *Chemical physics letters* **221**, 100 (1994).
 - [7] V. Hrouda, M. Roeselova, and T. Bally, *The Journal of Physical Chemistry A* **101**, 3925 (1997).
 - [8] S. Patchkovskii, J. Autschbach, and T. Ziegler, *The Journal of chemical physics* **115**, 26 (2001).
 - [9] P. Mori-Sánchez, A. J. Cohen, and W. Yang, *Physical review letters* **100**, 146401 (2008).
 - [10] C. Toher and S. Sanvito, *Physical Review B—Condensed Matter and Materials Physics* **77**, 155402 (2008).
 - [11] Y. Zhang, J. Furness, R. Zhang, Z. Wang, A. Zunger, and J. Sun, *Physical Review B* **102**, 045112 (2020).
 - [12] Y. Zhang, J. W. Furness, B. Xiao, and J. Sun, *The Journal of chemical physics* **150** (2019).
 - [13] R. Zhang, B. Singh, C. Lane, J. Kidd, Y. Zhang, B. Barbiellini, R. S. Markiewicz, A. Bansil, and J. Sun, *Physical Review B* **105**, 195134 (2022).
 - [14] H. C. Fitzhugh, J. W. Furness, M. R. Pederson, J. E. Peralta, and J. Sun, *Journal of Chemical Theory and Computation* **19**, 5760 (2023).
 - [15] M. R. Pederson, A. Ruzsinszky, and J. P. Perdew, *The Journal of Chemical Physics* **140** (2014).
 - [16] R. R. Zope, Y. Yamamoto, C. M. Diaz, T. Baruah, J. E. Peralta, K. A. Jackson, B. Santra, and J. P. Perdew, *The Journal of Chemical Physics* **151** (2019).
 - [17] M. R. Pederson, A. Ruzsinszky, and J. P. Perdew, *The Journal of Chemical Physics* **140** (2014).
 - [18] C. Li, X. Zheng, N. Q. Su, and W. Yang, *National Science Review* **5**, 203 (2018).

- [19] A. Mahler, J. Williams, N. Q. Su, and W. Yang, *Physical Review B* **106**, 035147 (2022).
- [20] J. P. Perdew, V. Staroverov, J. Tao, and G. E. Scuseria, *Phys. Rev. A* **78**, 052513 (2008).
- [21] J. Kirkpatrick, B. McMorrow, D. H. Turban, A. L. Gaunt, J. S. Spencer, A. G. Matthews, A. Obika, L. Thiry, M. Fortunato, D. Pfau, *et al.*, *Science* **374**, 1385 (2021).
- [22] M. Haasler, T. M. Maier, R. Grotjahn, S. Gückel, A. V. Arbuznikov, and M. Kaupp, *J. Chem. Theory Comput.* **16**, 5645 (2020).
- [23] A. D. Becke, *J. Chem. Phys.* **138**, 074109 (2013).
- [24] B. G. Janesko, *J. Chem. Phys.* **133**, 104103 (2010).
- [25] J. Kong and E. Proynov, *J. Chem. Theory Comput.* **12**, 133 (2015).
- [26] J. Sun, A. Ruzsinszky, and J. P. Perdew, *Phys. Rev. Lett.* **115**, 036402 (2015).
- [27] J. P. Perdew, K. Burke, and M. Ernzerhof, *Physical review letters* **77**, 3865 (1996).
- [28] J. Sun, R. C. Remsing, Y. Zhang, Z. Sun, A. Ruzsinszky, H. Peng, Z. Yang, A. Paul, U. Waghmare, X. Wu, *et al.*, *Nature chemistry* **8**, 831 (2016).
- [29] U. Von Barth and L. Hedin, *Journal of Physics C: Solid State Physics* **5**, 1629 (1972).
- [30] J. P. Perdew and Y. Wang, *Physical review B* **45**, 13244 (1992).
- [31] A. D. Becke, *Physical review A* **38**, 3098 (1988).
- [32] J. P. Perdew, J. A. Chevary, S. H. Vosko, K. A. Jackson, M. R. Pederson, D. J. Singh, and C. Fiolhais, *Physical review B* **46**, 6671 (1992).
- [33] J. P. Perdew, S. Kurth, A. c. v. Zupan, and P. Blaha, *Phys. Rev. Lett.* **82**, 2544 (1999).
- [34] J. Tao, J. P. Perdew, V. N. Staroverov, and G. E. Scuseria, *Phys. Rev. Lett.* **91**, 146401 (2003).
- [35] J. Sun, B. Xiao, and A. Ruzsinszky, *The Journal of chemical physics* **137** (2012).
- [36] J. W. Furness, A. D. Kaplan, J. Ning, J. P. Perdew, and J. Sun, *The journal of physical chemistry letters* **11**, 8208 (2020).
- [37] D. Mejia-Rodriguez and S. B. Trickey, *Phys. Rev. A* **96**, 052512 (2017).
- [38] D. Mejia-Rodríguez and S. Trickey, *Physical Review B* **102**, 121109 (2020).
- [39] A. D. Kaplan and J. P. Perdew, *Physical Review Materials* **6**, 083803 (2022).
- [40] T. Lebeda, T. Aschebrock, and S. Kümmel, *Physical Review Letters* **133**, 136402 (2024).
- [41] A. D. Kaplan, M. Levy, and J. P. Perdew, *Annual Review of Physical Chemistry* **74**, 193 (2023).
- [42] J. Sun, B. Xiao, Y. Fang, R. Haunschield, P. Hao, A. Ruzsinszky, G. I. Csonka, G. E. Scuseria, and J. P. Perdew, *Physical review letters* **111**, 106401 (2013).
- [43] D. Mejia-Rodriguez and S. Trickey, *Physical Review B* **98**, 115161 (2018).
- [44] G. L. Oliver and J. P. Perdew, *Phys. Rev. A* **20**, 397 (1979).
- [45] J. P. Perdew and S. Kurth, in *A primer in density functional theory* (Springer, 2003) pp. 1–55.
- [46] J. P. Perdew, A. Ruzsinszky, J. Sun, and K. Burke, *The Journal of chemical physics* **140** (2014).
- [47] M. Levy, *Physical Review A* **43**, 4637 (1991).
- [48] R. F. Bader, *Accounts of chemical research* **18**, 9 (1985).
- [49] L. Hou, T. J. Irons, Y. Wang, J. W. Furness, A. M. Wibowo-Teale, and J. Sun, *The Journal of Chemical Physics* **160** (2024).
- [50] L. Hou, T. J. Irons, Y. Wang, J. W. Furness, A. M. Wibowo-Teale, and J. Sun, *The Journal of Physical Chemistry A* (2024).

Supplementary Material: How Semilocal Are Semilocal Density Functional Approximations?

—Tackling Self-Interaction Error in One-Electron Systems

Akilan Ramasamy,¹ Lin Hou,^{1,2} Jorge Vega Bazantes,¹ Tom J. P. Irons,³ Andrew M. Wibowo-Teale,^{3,4} and Jianwei Sun^{1,*}

¹*Department of Physics and Engineering Physics, Tulane University, New Orleans, Louisiana 70118, USA*

²*Theoretical Division, Los Alamos National Laboratory, Los Alamos, New Mexico 87545, USA*

³*School of Chemistry, University of Nottingham, University Park, Nottingham NG7 2RD, United Kingdom*

⁴*Hylleraas Centre for Quantum Molecular Sciences, Department of Chemistry, University of Oslo, P.O. Box 1033, N-0315 Oslo, Norway*

(Dated: November 22, 2024)

I. COMPUTATIONAL DETAILS

For parameter optimization, we used the Sequential Least Squares Programming (SLSQP) [1] algorithm from the SciPy [2] library. This algorithm offers the advantage of handling non-linear constraints, which is essential for satisfying the appropriate norms in our functional design. Specifically, we imposed a non-linear constraint to exactly recover the exchange energy of hydrogen, -0.3125 Ha. Additionally, the form of the functional was optimized to minimize the loss function for the Gaussian electron density. The loss function used for the Gaussian electron density is defined as,

$$\mathcal{L}^G = (E_x^{\text{RS}} - E_x^{\text{Exact}})^2, \quad (\text{S1})$$

where, \mathcal{L}^G represents the loss for the Gaussian density, E_x^{RS} is the exchange energy using the RS functional, and E_x^{Exact} is the exact exchange energy of gaussian, which is -0.3989 Ha. This approach ensures that our functional is accurately constrained for both hydrogen and Gaussian densities, providing a robust optimization framework.

All H_2^+ calculations were performed using Psi4 [3]. The Hartree-Fock (HF) electron density and total energy were computed using the cc-pV5Z basis set from the Dunning family [4–6], with the basis functions in their uncontracted spherical Gaussian form. This HF density was then used in a non-self-consistent manner to evaluate the exchange energies for various density functionals discussed in the main text. The binding energy curves for H_2^+ were generated based solely on the exchange energies, excluding the correlation energy contributions for all the functionals considered.

The computational procedures for both the Hartree-Fock exact exchange hole and the PBE exchange hole model largely follow the methodologies described in Refs. [7, 8], with calculations performed using the QUEST code [9]. The PBE exchange hole model employed the

Hartree-Fock electronic density and its gradient, and a spin-unrestricted formalism was adopted throughout to extend the analysis to single-electron states.

Spherically-averaged exchange holes were constructed via angular integration, using an order-41 Lebedev quadrature grid at each reference point [10, 11]. The PBE exchange hole model [12] were computed with a spatial sampling interval of 0.01 bohr for the interelectronic distance u .

II. DENSITY INGREDIENTS PLOTTED FOR DIFFERENT SYSTEMS

The density ingredients used in RS, s and q are plotted against position, r for the appropriate norms used, hydrogen density and gaussian density in Figure S1.

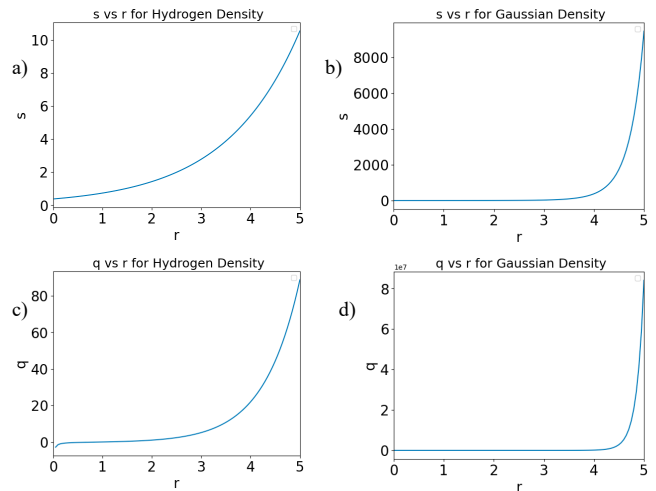


Figure S1. a) s vs r for hydrogen , b) s vs r for Gaussian electron density, c) q vs r for hydrogen, d) q vs r for Gaussian electron density (Note: Different scales are used for hydrogen and gaussian electron densities)

* Correspondence email address: jsun@tulane.edu

As the bond length of H_2^+ increases, the electron becomes progressively more delocalized, leading to a signif-

icant reduction in electron density around the bond center. This trend is clearly illustrated in Figure S2, where the electron density diminishes as the nuclei move apart.

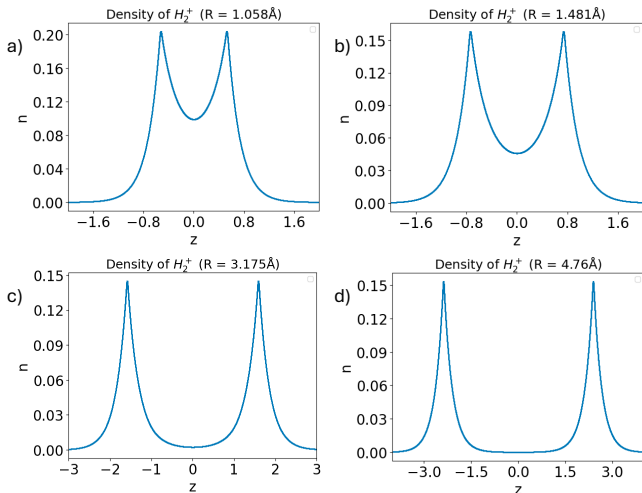


Figure S2. a) Electron density plotted against z for $R = 1.058\text{\AA}$, b) Electron density plotted against z for $R = 1.481\text{\AA}$, c) Electron density plotted against z for $R = 3.175\text{\AA}$, d) Electron density plotted against z for $R = 4.76\text{\AA}$

At critical points, such as bond centers, the reduced electron density gradient, s consistently remains zero, regardless of the bond length, R . However, the evolution of s along the bond axis, z varies as the bond length changes. Figure S3 illustrates how s behaves in the direction of the bond for different bond lengths.

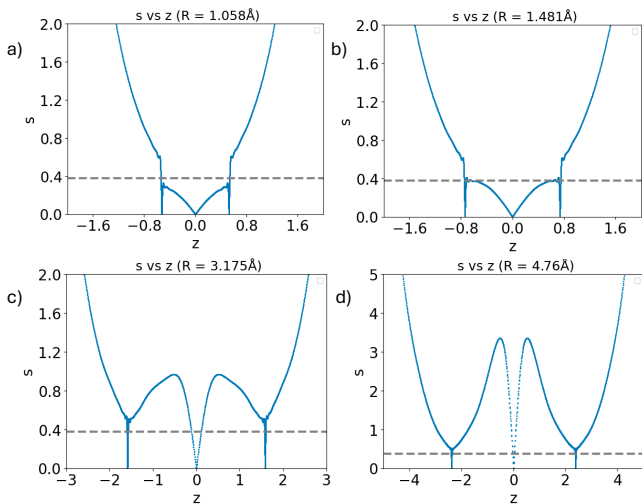


Figure S3. a) Reduced electron density gradient, s plotted against z for $R = 1.058\text{\AA}$, b) Reduced electron density gradient, s plotted against z for $R = 1.481\text{\AA}$, c) Reduced electron density gradient, s plotted against z for $R = 3.175\text{\AA}$, d) Reduced electron density gradient, s plotted against z for $R = 4.76\text{\AA}$

According to Bader's analysis [13] as discussed in the

main text, the reduced electron density Laplacian, q becomes increasingly positive as the electron density decreases, highlighting regions where the electron distribution is more diffuse. At the nuclear centers, q diverges to $-\infty$, indicating the highly localized nature of the electron density in these regions. Figure S4 illustrates the behavior of q along the bond axis, z for different bond lengths. As the bond length increases, the electron density spreads out, leading to a corresponding rise in q at the bond center.

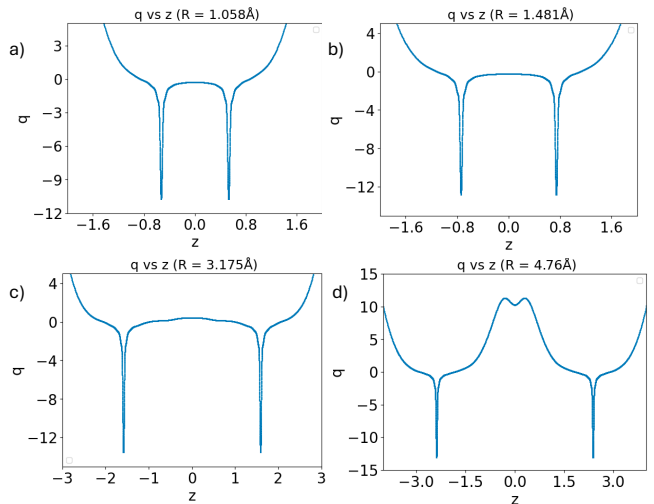


Figure S4. a) Reduced electron density Laplacian, q plotted against z for $R = 1.058\text{\AA}$, b) Reduced electron density Laplacian, q plotted against z for $R = 1.481\text{\AA}$, c) Reduced electron density Laplacian, q plotted against z for $R = 3.175\text{\AA}$, d) Reduced electron density Laplacian, q plotted against z for $R = 4.76\text{\AA}$

III. NON-UNIFORM COORDINATE SCALING

Electron density and Kohn-Sham orbitals that are non-uniformly scaled in one dimension (consider x direction in this case) is given by [14],

$$n_{\lambda}^x(x, y, z) = \lambda n(u, y, z) \quad (\text{S2})$$

$$\phi_{i,\lambda}^x(x, y, z) = \lambda^{1/2} \phi_i(u, y, z) \quad (\text{S3})$$

where $u = \lambda x$. The reduced density gradient, s is defined as,

$$s = \frac{|\nabla n|}{2(3\pi^2)^{1/3} n^{4/3}} \quad (\text{S4})$$

Here, we define another dimensionless quantity $p = s^2$ for the simplicity of illustrating the scaling of s at the limits. When p is non-uniformly scaled along x direction, the dimensionless gradient p can be expressed as [14]

$$p_\lambda^x(x, y, z) = \frac{1}{4(3\pi^2)^{2/3}n(u, y, z)^{8/3}} \left(\lambda^{4/3} f_{p1}(u, y, z) + \lambda^{-2/3} f_{p2}(u, y, z) \right) \quad (\text{S5})$$

where,

$$f_{p1}(u, y, z) = \left[\frac{\partial n(u, y, z)}{\partial u} \right]^2 \quad (\text{S6})$$

$$f_{p2}(u, y, z) = |\nabla_\perp n(u, y, z)|^2 \quad (\text{S7})$$

When $\lambda \rightarrow 0$, p will scale as $\lambda^{-2/3}$ and hence s will scale as $\lambda^{-1/3}$. Similarly, when $\lambda \rightarrow \infty$, p will scale as $\lambda^{4/3}$ and s will scale as $\lambda^{2/3}$.

Similarly, we can define the reduced density laplacian, q as

$$q = \frac{\nabla^2 n}{4(3\pi^2)^{2/3}n^{5/3}} \quad (\text{S8})$$

When q is non-uniformly scaled along x direction, it can be expressed as,

$$q_\lambda^x(x, y, z) = \frac{1}{4(3\pi^2)^{2/3}n(u, y, z)^{5/3}} \left(\lambda^{4/3} f_{q1}(u, y, z) + \lambda^{-2/3} f_{q2}(u, y, z) \right) \quad (\text{S9})$$

where,

$$f_{q1}(u, y, z) = \frac{\partial^2 n(u, y, z)}{\partial u^2} \quad (\text{S10})$$

$$f_{q2}(u, y, z) = \nabla_\perp^2 n(u, y, z) \quad (\text{S11})$$

When $\lambda \rightarrow 0$, q scales as $\lambda^{-2/3}$. In contrast, for $\lambda \rightarrow \infty$, q scales as $\lambda^{4/3}$. In the latter case, q may diverge to either $-\infty$ or $+\infty$, depending on the sign of $f_{q1}(u, y, z)$. Near or at the nucleus, where the second derivative of the density with respect to position u ($f_{q1}(u, y, z)$) is negative, q tends toward $-\infty$ as $\lambda \rightarrow \infty$. Conversely, in other regions where $f_{q1}(u, y, z)$ is positive, q tends toward $+\infty$. Figure S5 illustrates these limiting behaviors for q as $\lambda \rightarrow \infty$, using the non-uniformly scaled hydrogen (NUSH) density [15], with q expressed in cylindrical coordinates (u and ρ).

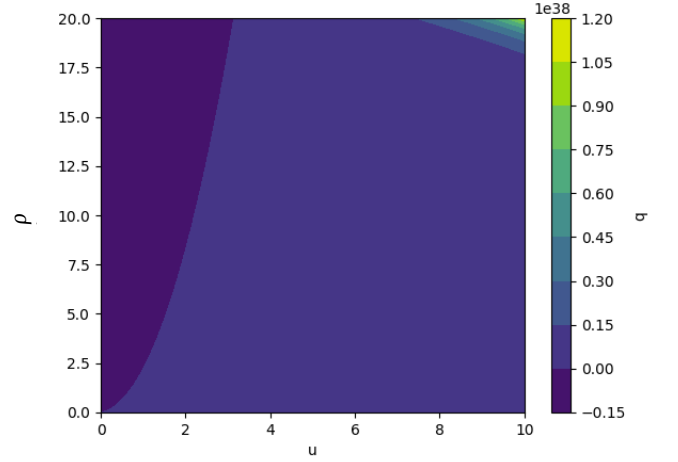


Figure S5. Contour plot of q_λ^x against u and ρ for $\lambda = 10^{20}$

As shown in the figure, for a large positive value of λ (e.g., 10^{20}), the value of q scales down to approximately -10^{38} in the smaller u regions, while in other regions, it scales up to around $+10^{38}$.

The analytical expressions for the electron density, n , spin-scaled s and q derived for NUSH are given below,

$$n_\lambda^x(r) = \frac{\lambda e^{-2\sqrt{(\lambda x)^2 + y^2 + z^2}}}{\pi} \quad (\text{S12})$$

$$s[2n_\lambda^x] = \frac{\sqrt{\lambda^2 \left(\frac{\partial r_u}{\partial u} \right)^2 + \left(\frac{\partial r_u}{\partial y} \right)^2 + \left(\frac{\partial r_u}{\partial z} \right)^2}}{(6\pi^2)^{1/3} (n_\lambda^x)^{1/3}} \quad (\text{S13})$$

where $r_u = (u^2 + y^2 + z^2)^{1/2}$

$$q[2n_\lambda^x] = \frac{w(u, y, z, r_u, \lambda)}{4(6\pi^2)^{2/3} (n_\lambda^x)^{2/3}} \quad (\text{S14})$$

where,

$$w(u, y, z, r_u, \lambda) = 2\lambda^2 \left(\frac{2u^2}{r_u^2} - \frac{1}{r_u} + \frac{u^2}{r_u^3} \right) + 2 \left(\frac{2y^2}{r_u^2} - \frac{1}{r_u} + \frac{y^2}{r_u^3} \right) + 2 \left(\frac{2z^2}{r_u^2} - \frac{1}{r_u} + \frac{z^2}{r_u^3} \right) \quad (\text{S15})$$

IV. DERIVATION OF THE EXACT SYSTEM- AND SPHERICALLY-AVERAGED EXCHANGE HOLE

The analytic expression of the exact system- and spherically-averaged exchange holes of the Hydrogenic and Gaussian electron densities can be derived.

For one-electron systems,

$$n_x(\mathbf{r}, \mathbf{r}+\mathbf{u}) = -n(\mathbf{r}+\mathbf{u}). \quad (\text{S16})$$

A. Hydrogenic density

Let us consider the normalized hydrogenic 1s orbital density:

$$n^H(\mathbf{r}) = \frac{\alpha^3}{8\pi} e^{-\alpha r} \quad (\text{S17})$$

and find the spherically averaged exchange-hole function $n_x^H(\mathbf{r}, u)$ written as:

$$n_x^H(\mathbf{r}, u) = -\frac{1}{4\pi} \int d\Omega_{\mathbf{u}} n^H(\mathbf{r} + \mathbf{u}). \quad (\text{S18})$$

Notice that $n_x^H(\mathbf{r}, u) = \frac{\alpha^3}{8\pi} e^{-\alpha|\mathbf{r}+\mathbf{u}|}$ and $|\mathbf{r} + \mathbf{u}| = \sqrt{r^2 + u^2 + 2ru\cos(\theta)}$. Then,

$$n_x^H(\mathbf{r}, u) = -\frac{1}{4\pi} \int d\Omega_{\mathbf{u}} \frac{\alpha^3}{8\pi} e^{-\alpha\sqrt{r^2+u^2+2ru\cos(\theta)}} \quad (\text{S19})$$

where the solid angle is $d\Omega_{\mathbf{u}} = \sin(\theta)d\theta d\phi$, with $\theta \in [0, \pi]$, and $\phi \in [0, 2\pi]$. Hence, after integrating we get:

$$n_x^H(\mathbf{r}, u) = -\frac{\alpha}{16\pi ru} \left((\alpha|r-u|+1)e^{-\alpha|r-u|} - (\alpha|r+u|+1)e^{-\alpha|r+u|} \right) \quad (\text{S20})$$

Next, we get the system- and spherically-averaged exchange hole $\langle n_x^H \rangle(u)$:

$$\begin{aligned} \langle n_x^H \rangle(u) &= \frac{1}{N} \int d\mathbf{r} n^H(\mathbf{r}) n_x^H(\mathbf{r}, u) \\ &= -\frac{1}{N} \int dr r^2 \sin(\theta) d\theta d\phi \left(\frac{\alpha^3}{8\pi} e^{-\alpha r} \right) \\ &\times \frac{\alpha}{16\pi ru} \left[(\alpha|r-u|+1)e^{-\alpha|r-u|} - (\alpha|r+u|+1)e^{-\alpha|r+u|} \right] \\ &= -\frac{\alpha^4}{32\pi Nu} \left(\frac{1}{6} u^2 e^{-\alpha u} (\alpha u + 3) \right. \\ &\quad \left. + \frac{e^{-\alpha u} (3\alpha u + 2)}{4\alpha^2} - \frac{e^{-\alpha u} (\alpha u + 2)}{4\alpha^2} \right) \end{aligned} \quad (\text{S21})$$

Then, since the exchange energy is given by

$$E_x = \int_0^\infty du 4\pi u^2 N \frac{\langle n_x^H \rangle(u)}{2u} \quad (\text{S22})$$

we can check the correctness of our previous expressions by integrating over u and setting $\alpha = 2Z$ where $Z = 1$ and $N = 1$ to get $E_x = -0.3125$ Ha.

B. Gaussian electron density

In the same way as done for the Hydrogenic density, now let us consider the Gaussian electron density:

$$n^G(r) = \frac{e^{-r^2}}{\pi^{3/2}}. \quad (\text{S23})$$

We can find the Gaussian spherically averaged exchange-hole function by:

$$n_x^G(\mathbf{r}, u) = -\frac{1}{4\pi} \int d\Omega_{\mathbf{u}} n^G(\mathbf{r} + \mathbf{u}) \quad (\text{S24})$$

$$= -\frac{1}{4\pi} \int d\theta \sin(\theta) d\phi \frac{e^{-|r+u|^2}}{\pi^{3/2}} \quad (\text{S25})$$

$$= -\frac{1}{2\pi^{3/2}ru} e^{-(r^2+u^2)} \sinh(2ru) \quad (\text{S26})$$

Next, we can get the system- and spherically-averaged exchange hole $\langle n_x^G \rangle(u)$:

$$\langle n_x^G \rangle(u) = \frac{1}{N} \int d\mathbf{r} n^G(\mathbf{r}) n_x^G(\mathbf{r}, u) \quad (\text{S27})$$

$$= -\left(\frac{1}{N} \right) \frac{e^{-\frac{u^2}{2}}}{2\sqrt{2}\pi^{3/2}} \quad (\text{S28})$$

Finally the exchange energy is obtained by integrating over u and setting $N = 1$:

$$E_x = \int_0^\infty du 4\pi u^2 N \frac{\langle n_x^G \rangle(u)}{2u} = -0.3989 \text{ Ha} \quad (\text{S29})$$

which confirms the consistency of the previous equations and the end of these proofs.

V. THE DEVIATIONS OF PBE EXCHANGE HOLES FROM THE EXACT ONES IN THE ONE-ELECTRON SYSTEMS

Figure S6 plots the difference of PBE and exact system- and spherically-averaged exchange holes weighted by the inter-electron distance u . The integration of the above difference yields the deviation of PBE exchange energy from the exact one. It can be seen for all the considered systems that the PBE exchange holes are deeper in the short range than the exact ones, resulting in being shallower in the longer range due to the sum rule. For H and H_2^+ at small bond lengths ($R \leq 1.058\text{\AA}$), the exact exchange hole is deep, and the overestimation in depth from the PBE exchange hole in the short range is small, followed by a localized peak representing an underestimation in hole depth. The cancellation between the well and the peak results in reasonably good accuracy for the exchange energies, for example, of H (-0.3059 Ha of PBE vs -0.3125 Ha of exact), although the PBE exchange hole was derived by enforcing the sum rule on the exchange hole of slowly varying densities [12]. When the bond length R increases, the exact exchange hole becomes shallower as shown in Figure S6 while the PBE exchange hole becomes too deep, leading to too negative exchange energies and large SIE, as shown in Figure 1 in the main text.

Since SCAN satisfies exact constraints for one-electron systems that PBE does not and improves upon PBE in exchange energies, it is reasonable to believe that a properly reverse-engineered SCAN exchange hole model could

provide shallower exchange holes than PBE, though still deeper than the exact ones.

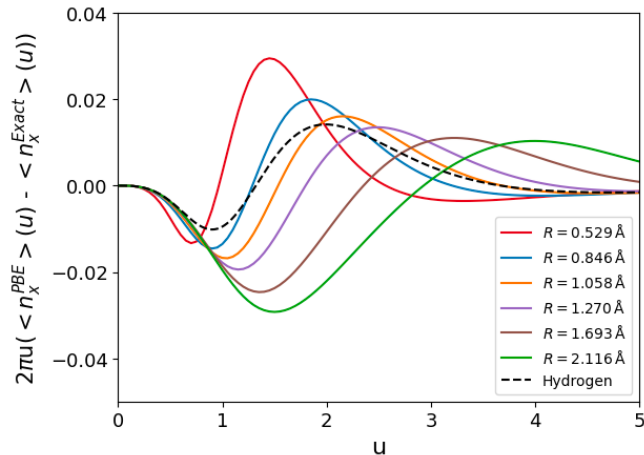


Figure S6. Difference between exact and the PBE system- and spherically-averaged exchange hole multiplied by $2\pi u$ plotted against u

VI. DERIVATION OF $q_H(s)$

Let's substitute $\alpha = 2Z$ and $Z = 1$ in Eq. S17, the electron density for a hydrogen atom is then given by

$$n^H(r) = \frac{e^{-2r}}{\pi}. \quad (\text{S30})$$

The spin-scaled reduced density gradient, s , can be derived from Eq. S4, scaled by a factor of $\frac{1}{2^{1/3}}$ due to the spin scaling, and is expressed as

$$s^H(r) = \frac{e^{-2r}}{(e^{-2r})^{4/3}(6\pi)^{1/3}}, \quad (\text{S31})$$

while the spin-scaled reduced electron density Laplacian, q , follows from Eq. S8 and is given by

$$q^H(r) = \frac{e^{4r/3} \left(1 - \frac{1}{r}\right)}{(6\pi)^{2/3}}. \quad (\text{S32})$$

From Eq. S31, r can be expressed in terms of s as

$$r = \frac{3}{2} \ln \left((6\pi)^{1/3} s \right). \quad (\text{S33})$$

Substituting Eq.S33 into Eq.S32, q can then be expressed as a function of s , yielding the following relationship:

$$q_H(s) = \left[1 - \frac{2}{3 \ln \left((6\pi)^{1/3} s \right)} \right] s^2. \quad (\text{S34})$$

This formulation allows for $q_H(s)$ to be computed directly in terms of the reduced density gradient s for the hydrogen atom.

VII. MORE CONTOUR PLOTS OF $F_x^{RS} - F_x^{SCAN}$

As bond lengths increases, more (s, q) points appear above $q_0(s)$, leading to improved energy descriptions compared to SCAN. To illustrate this, the (s, q) points at $R = 2.116 \text{ \AA}$ are plotted against the difference in enhancement factors between RS and SCAN in Figure S7, in comparison with the plot of $R = 1.058 \text{ \AA}$ shown in Figure 4(a) of the main text. Notably, for regions where $s > 1$, a great number of data points lie above $q_0(s)$, resulting in a significantly smaller F_x value relative to SCAN. This reduction in F_x contributes to a more accurate energy description for H_2^+ , improving the overall binding energy curve.

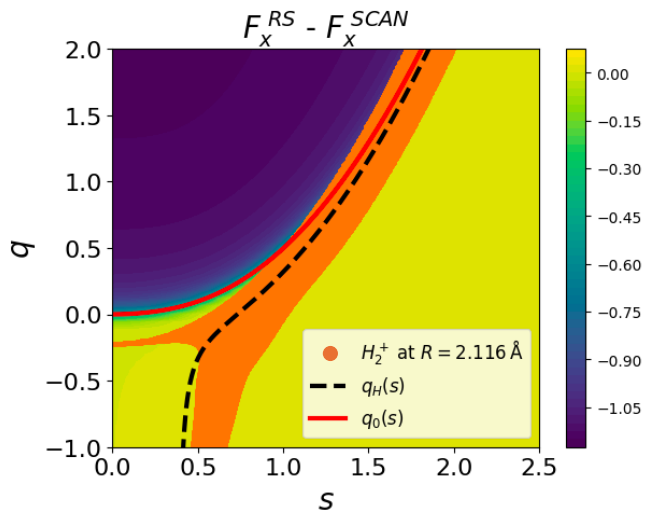


Figure S7. Contour Plot of the difference in the RS and SCAN enhancement factors against s and q , overlaid by (s, q) points existing in H_2^+ with bond length $R = 2.116 \text{ \AA}$.

[1] D. Kraft, Forschungsbericht- Deutsche Forschungs- und Versuchsanstalt für Luft- und Raumfahrt (1988).

[2] P. Virtanen, R. Gommers, T. E. Oliphant, M. Haberland, T. Reddy, D. Cournapeau, E. Burovski, P. Pe-

- terson, W. Weckesser, J. Bright, S. J. van der Walt, M. Brett, J. Wilson, K. J. Millman, N. Mayorov, A. R. J. Nelson, E. Jones, R. Kern, E. Larson, C. J. Carey, Í. Polat, Y. Feng, E. W. Moore, J. VanderPlas, D. Laxalde, J. Perktold, R. Cimrman, I. Henriksen, E. A. Quintero, C. R. Harris, A. M. Archibald, A. H. Ribeiro, F. Pedregosa, P. van Mulbregt, and SciPy 1.0 Contributors, *Nature Methods* **17**, 261 (2020).
- [3] J. M. Turney, A. C. Simmonett, R. M. Parrish, E. G. Hohenstein, F. A. Evangelista, J. T. Fermann, B. J. Mintz, L. A. Burns, J. J. Wilke, M. L. Abrams, *et al.*, Wiley Interdisciplinary Reviews: Computational Molecular Science **2**, 556 (2012).
- [4] T. H. Dunning, *J. Chem. Phys.* **90**, 1007 (1989).
- [5] D. E. Woon and T. H. Dunning, *J. Chem. Phys.* **98**, 1358 (1993).
- [6] D. E. Woon and T. H. Dunning, *J. Chem. Phys.* **103**, 4572 (1995).
- [7] L. Hou, T. J. Irons, Y. Wang, J. W. Furness, A. M. Wibowo-Teale, and J. Sun, *J. Chem. Phys.* **160**, 014103 (2024).
- [8] L. Hou, T. J. Irons, Y. Wang, J. W. Furness, A. M. Wibowo-Teale, and J. Sun, *The Journal of Physical Chemistry A* (2024).
- [9] “QUEST, a rapid development platform for QUantum Electronic Structure Techniques,” <https://quest.codes/> (2024).
- [10] V. Lebedev, *USSR Computational Mathematics and Mathematical Physics* **16**, 10 (1976).
- [11] V. I. Lebedev and A. L. Skorokhodov, *Doklady Akademii Nauk* **324**, 519 (1992).
- [12] M. Ernzerhof and J. P. Perdew, *The Journal of Chemical Physics* **109**, 3313 (1998), https://pubs.aip.org/aip/jcp/article-pdf/109/9/3313/19115007/3313_1_online.pdf.
- [13] R. F. Bader, *Accounts of chemical research* **18**, 9 (1985).
- [14] J. W. Furness, A. D. Kaplan, J. Ning, J. P. Perdew, and J. Sun, *The Journal of Chemical Physics* **156** (2022).
- [15] S. Kurth, *Journal of Molecular Structure: THEOCHEM* **501**, 189 (2000).